Fast growth of monolayer organic 2D crystals and their application in organic transistors

Wang, Zhifang; Niu, Xiaona; Zhou, Xu; Song, Ruxin; Wang, Zi; Huang, Lizhen; Chi, Lifeng

Published in:
Organic Electronics

DOI:
10.1016/j.orgel.2018.03.038

Publication date:
2018

Organic Electronics 58 (2018) 38–45

Contents lists available at ScienceDirect

Organic Electronics

journal homepage: www.elsevier.com/locate/orgel

Fast growth of monolayer organic 2D crystals and their application in organic transistors

Zhifang Wang[a], Xiaona Niu[a], Xu Zhou[a], Ruxin Song[a], Zi Wang[a,b], Lizhen Huang[a,*], Lifeng Chi[a,**]

[a] Jiangsu Key Laboratory for Carbon-Based Functional Materials & Devices, Institute of Functional Nano & Soft Materials (FUNSOM), Joint International Research Laboratory of Carbon-Based Functional Materials and Devices, Soochow University, 199 Ren'ai Road, Suzhou, 215123, Jiangsu, PR China

[b] Zernike Institute for Advanced Materials, Faculty of Science and Engineering, University of Groningen, Nijenborgh 4, 9747 AG, Groningen, The Netherlands

ARTICLE INFO

Keywords:
Organic thin film transistor
2D molecular crystals
Organic semiconductor
Dip coating

ABSTRACT

Growth of monolayer 2D organic crystal has been an interesting topic in recent years owing to their promising properties. However, it is still a tough challenge to obtain the 2D organic crystal with precise thickness control and uniform morphology. Herein, we reported the fabrication of 2D crystals of alkane molecules $C_{44}H_{90}$ with only monolayer thickness and tunable size through the simple dip-coating process. Benefitted from the low solubility of the $C_{44}H_{90}$ and the isotropic Van der Waals interaction, quadrilateral-shape monolayer 2D crystals with size from several micrometers to nearly hundreds of micrometers can be achieved in the dip-coating process. Utilized the X-ray diffraction and high resolution atomic force microscopy, we obtained the clear packing mode of these monolayer crystals. In addition, these smooth 2D crystals show promising application in the thin film transistors by acting as a molecular template layer. It leads to an increment of about one magnitude on the charge mobility owing to the decreasing of both morphology defects and interface traps.

1. Introduction

Growth of high quality organic micro- or nanocrystals has been a hot topic over long time due to their wide applications in e.g. molecular electronics, non-linear optics, pigments and dyes, pharmaceutical drug delivery [1–9]. Specifically, along with the fast development of inorganic two-dimensional (2D) materials [10–12], the low dimensional organic crystals in 2D or one-dimensional (1D) turn to be highly interesting, especially owing to their promising unique properties in optoelectronics. A number of strategies has been developed for the preparation of ordered 2D or 1D molecular crystals [4–9]. Typical techniques include solution shearing, dip-coating, drop-casting, slot-die coating and template assisting methods [13–33]. Using those approaches, highly ordered crystals specifically the 1D stripe-like crystals were achieved. Li et al. reported the fast fabrication of micro-stripes crystals of dithieno [2,3-d; 2′,3′-d′]benzo-[1,2-b; 4,5-b′]dithiophene (DTBDT) derivative utilized the dip-coating technique and demonstrated their promising applications as high sensitive gas sensors [25,34]. Bao et al. produced highly aligned organic crystals by the solution shearing technique and obtained high mobility transistors [13].

Compare to the 1D crystals, growing 2D molecular crystals with controllable morphology and precise thickness is relatively a tough challenge [3,9,35,36]. Jiang et al. reported the fabrication of millimeter-sized monolayer 2D crystals, which possess mobility up to 1 $cm^2V^{-1}s^{-1}$ through drop-coating method [36]. Utilizing the floating-coffee-ring driven assembly method, Wang et al. realized the large-scale 2D organic crystal with precise thickness control [9]. Here we report a simple method for fast growing 2D molecular crystals with a precise monolayer thickness. By the simple dip-coating method, we can achieve a series of monolayer molecular crystals with tailoring size from several micrometers to hundreds of micrometers. In addition, these crystals with the ultrathin and smooth features displayed promising applications in the organic electronic device through acting as template layers.

2. Experimental section

2.1. Materials and film fabrication

Tetratetracontane ($C_{44}H_{90}$) (> 97.0%) in our experimental was purchased from TCI and used without further purification. It was dissolved in n-heptane (anhydrous, > 99.0%, purchased from Alfa Aesar) to form solution with concentration of 0.97 mmol/L. The silicon wafer with 300 nm SiO_2 layer (C_i = 10 nF cm^{-2}) as substrate was immersed into the solution and then was pulled out at different speed ranging

* Corresponding author.
** Corresponding author.
E-mail addresses: chilf@suda.edu.cn (L. Huang), lzhuang@suda.edu.cn (L. Chi).

https://doi.org/10.1016/j.orgel.2018.03.038
Received 26 February 2018; Received in revised form 19 March 2018; Accepted 21 March 2018
Available online 26 March 2018

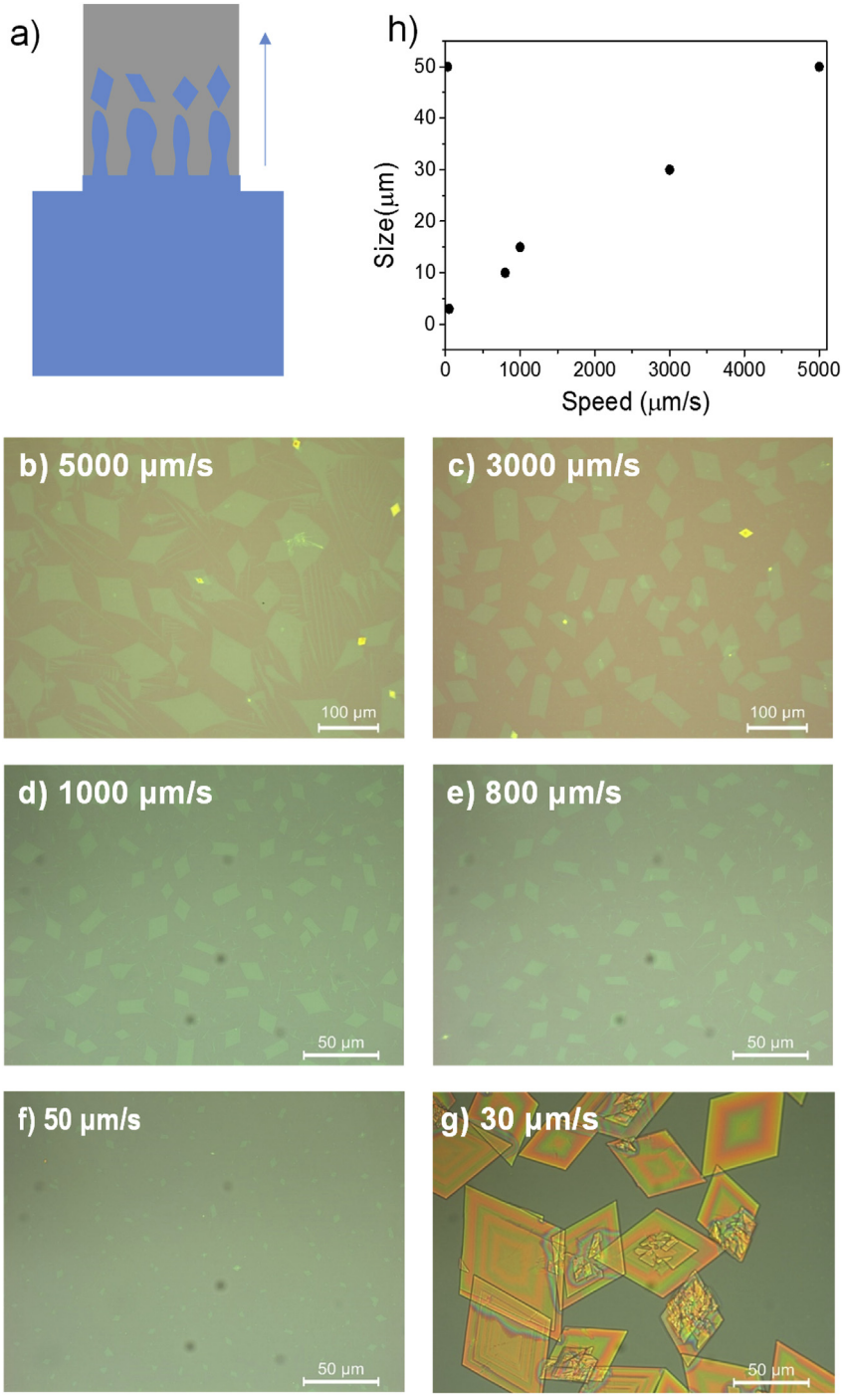

Fig. 1. a) the schematic diagram of dip-coating, b-g) optical microscopy image of $C_{44}H_{90}$ crystal prepared at different pulling speed, h) plots of the average crystal size vs withdrawal speed.

from 30 to 5000 μm/s during the process of dip-coating. Then pentacene was deposited on the surface of tetratetracontane thin film through vacuum deposition. The substrate temperature was 40 °C and the deposition rate was 0.1–0.5 nm/min. The experiments were performed at laboratory condition of which the temperature and humidity were 18.0–29.0 °C and 28.0–68.0%, respectively.

2.2. Thin film characterization

Optical topography of thin film was obtained on a Leica optical microscopy. Morphology, thickness, and width were measured with atomic force microscopy (AFM) using a Bruker Dimensional Icon in tapping mode.

2.3. Device fabrication and characterization

Gold source and drain electrodes (40 nm) were deposited through a shadow mask on top of the pentacene film by using thermal evaporator in Glove box (MIKROUNA Company) to form the bottom gate top contact OFETs. The electrical properties were measured in air with a Keithley 4200SCS semiconductor parameter analyser integrated with a probe station of Model 8060 from Micromanipulator Co., Inc.

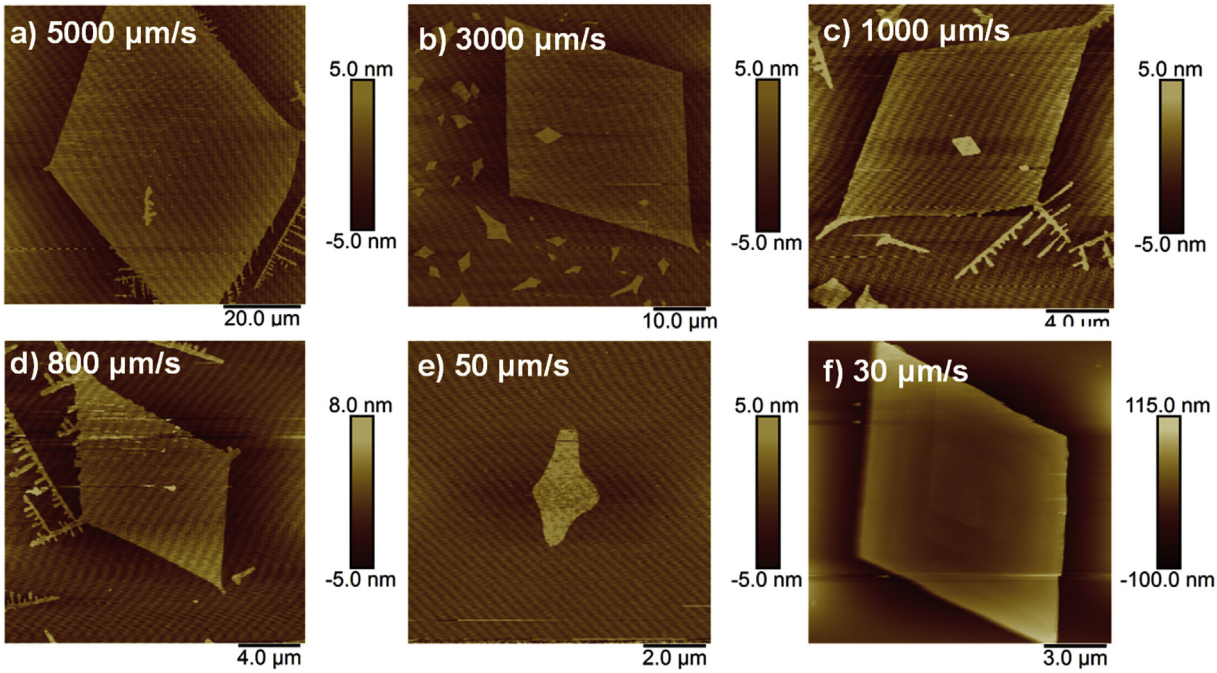

Fig. 2. AFM height image of $C_{44}H_{90}$ crystals prepared at different pulling speed. a) 5000 μm/s, b) 3000 μm/s, c) 1000 μm/s, d) 800 μm/s, e)50 μm/s, f) 30 μm/s.

3. Results and discussions

3.1. Morphology and structure of $C_{44}H_{90}$ crystals

Fig. 1a illustrates the schematic demonstration of the dip-coating process. The silicon wafer was dipped into the $C_{44}H_{90}$/n-heptane solution and then pulled out at different speeds. Fig. 1b–g presents the optical microscopy images of the samples with pulling speeds from 5000 to 30 μm/s. In contrast to the continuous stripe or fiber-like morphology of many organic semiconductors films, the $C_{44}H_{90}$ formed into many scattered lamellar crystals with uniform thickness and diamond quadrilateral shape in all the speed range except the case of 30 μm/s. The crystal size exhibits an obvious speed dependent manner. Fig. 1h plots the size vs pulling speed, which indicates a nearly linear relationship when the speed is over 50 μm/s. Pulling at 5000 μm/s results in the formation of dozens of crystals with average size approximately 50 *50 μm^2 on the substrates (Fig. 1b). At the speed of 3000 μm/s, the size reduces to about 30*30 μm^2, while it is approximately 5*5 μm^2 at the speed of 50 μm/s. When the speed further reduces to 30 μm/s, in contrast, the obtained crystals increases strongly in size and thickness, suggesting the occurrence of a different growth behavior. In addition to the morphology differences, the distribution of the crystals also changed from a relatively uniform state at higher speeds (> 50 μm/s) to an obviously non-uniform at 30 μm/s according to the large scale images depicted in Fig. S1. Therefore, according to the morphology evolution, the crystallization process at 30 μm/s transits to a similar process of crystal growth in the solution environment. In addition, we can also observe some small quadrangular crystals or dendritic crystals randomly located among the large size 2D crystals when speed over 800 μm/s.

We further characterized the crystal morphology by the AFM, as shown in Fig. 2. From 5000 μm/s to 50 μm/s, the height of the ultrathin crystals is approximately 4.4 ± 0.3 nm (Fig. S2), which is relative smaller than the fully extended chain length of $C_{44}H_{90}$ (5.5 nm). This gives the evidence that the molecule adopts a slight tilted orientation. More importantly, it indicates that all the 2D crystals are only one monolayer thick. In other words, by this simple dip-coating approach, we can easily obtain the 2D monolayer crystals with tunable size and uniform distribution by adjusting the withdrawal speed. The large 3D crystals formed at 30 μm/s gave a thickness up to hundreds of nm, and presented several terraced steps, in accordance with the optical microscopy images.

To understand the formation of these crystals and the speed dependent morphology evolution, we need to look back for the mechanism of dip-coating technique. During this lifting-crystallizing process, the crystal morphology is critically related to the meniscus formed between the substrate and the solution. The height (the distance away from the solution surface) and thickness (thickness of the rising liquid film on the substrate) of this meniscus varies with the withdrawal speed. At low withdrawal speed (< 30 μm/s), the meniscus height is relative small and the crystallization is an evaporation driven process, which is similar to the crystal growth under equilibrium state. Here, considering the low solubility of $C_{44}H_{90}$ and fast evaporation of *n*-heptane, the crystal will grow fast not only in the meniscus area but also in the solution nearby and retain on the substrate after pulling out, resulting in the large size 3D crystals. At higher speed (> 50 μm/s), the meniscus will extend and the obtained crystals mainly form at the air-solution-substrates contact line, leading to the formation of 2D monolayer crystals. In this situation, the meniscus shape depends on competition between the liquid capillary force upward and the gravitational force downward, which is the typical regime II as illustrated in many previous reports [24,25,31,37].

The morphology of such ordered quadrangular crystals of $C_{44}H_{90}$ with only monolayer thickness is fascinating and unique as a 2D organic material. From morphologic view, these $C_{44}H_{90}$ 2D crystals present some different features from previous dip-coating films. Firstly, all crystals exhibit a uniform monolayer thickness feature, which is distinct from many organic semiconductor films which usually present a V-shape speed-dependent thickness. This monolayer thickness is consistent with the other alkane molecular film e.g. $C_{32}H_{66}$ reported previously by Patrick Huber et al. [31]. And such monolayer is mainly originated from the low concentration at the meniscus area. Here the low concentration of $C_{44}H_{90}$ (0.97 mmol/L) makes it insufficient to form multiple layers during the fast dip-coating process. Instead, the speed-dependent behavior is reflected in the 2D crystal coverage and size. Secondly, the regular quadrangular shape and discontinuous feature of the $C_{44}H_{90}$ is different from the $C_{32}H_{66}$ which presents dragonfly crystals in low speed and continuous stripe crystals in high speed. This

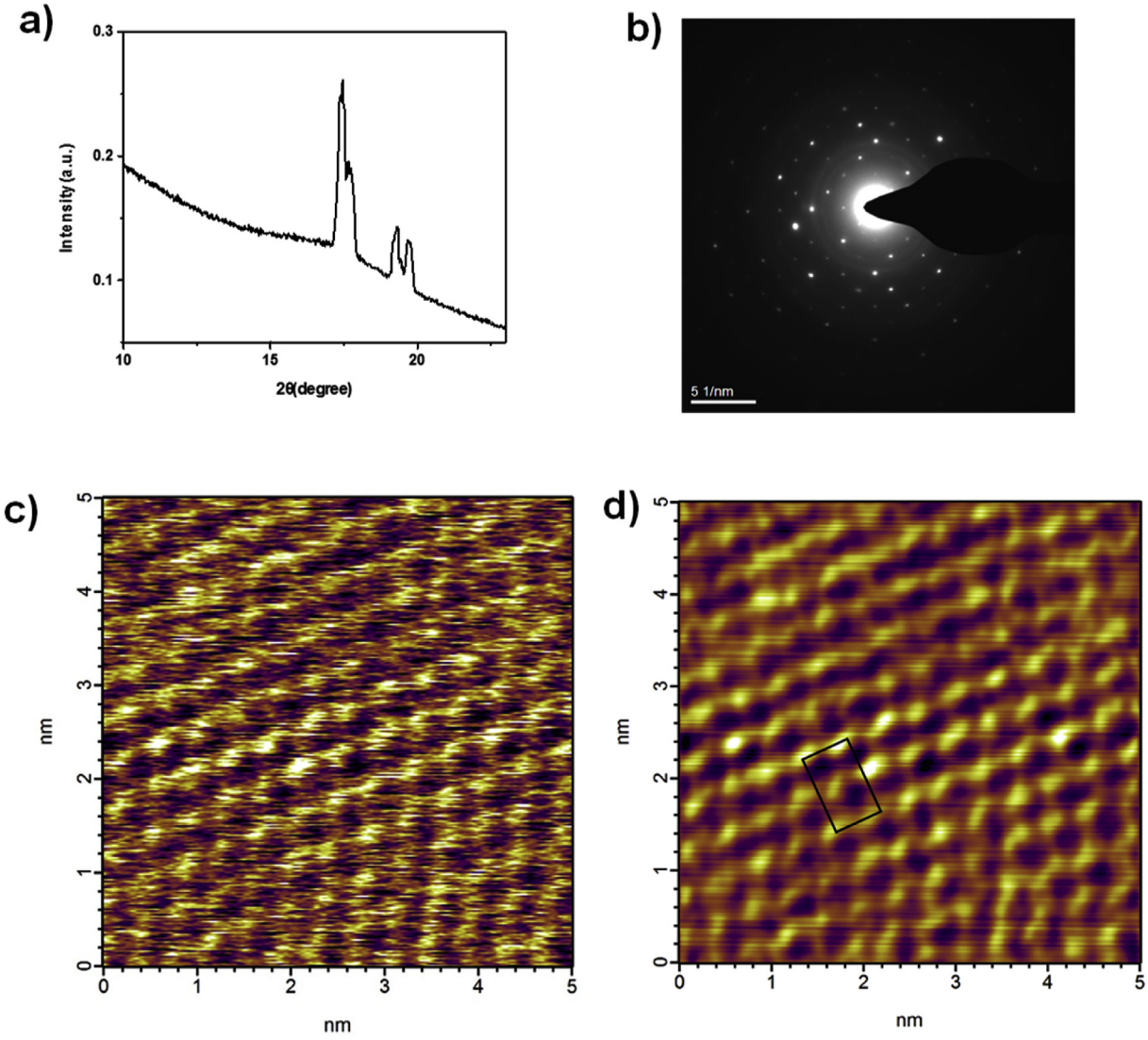

Fig. 3. a)GIXRD pattern of $C_{44}H_{90}$ crystals, b) the selected area electron diffraction. C) HRAFM of C44H90 crystal and the corresponding Fourier transformation image. The black rectangle marks the unit cell.

should relate to the low solubility of $C_{44}H_{90}$. On the meniscus, the solution develops into a supersaturated state quickly when the solvent evaporates, which leads to the appearance of a large number of nuclei. This nucleation of 2D crystal will deplete the surround solute molecules and generate a no-solute gap area. Accompanied by the Marangoi effect, the liquid meniscus will develop into discontinuous droplets along with the crystal growth and results in the scattered 2D monolayer crystals on the substrates [31,38,39].

The structure of the obtained 2D crystals was characterized with grazing incidence X-ray diffraction (GIXRD). Owing to the monolayer feature of the crystal, the out-of-plane diffraction is not possible to observe. The in-plane diffraction was recorded by the one-dimensional GIXRD utilizing the synchrotron radiation X-ray. Fig. 3a presents the obtained GIXRD pattern of $C_{44}H_{90}$ crystals. Three major diffraction features are presented: a major diffraction peak couple with a shoulder peak observed around the $2\theta = 15^{\circ}$ and two diffraction peaks around $2\theta = 20^{\circ}$. The calculated lattice spacing is 4.10 Å (4.01 Å), 3.70 Å and 3.60 Å respectively. This is quite similar to the orthorhombic crystal parameters reported previously of which the three diffraction corresponding to the (110), (020) and (021)respectively [40–43]. The selected area electronic diffraction indicates that the crystal only presents one set of in-plane diffraction, confirming the nearly single-crystal nature (Fig. 3b). In order to gain deep insight of the packing information, we performed high resolution AFM to characterize such monolayer crystals. As shown in Fig. 3c and d, the molecules arrange in a well-ordered manner. The packing mode is similar to the herringbone fashion and give a unit cell of a = 7.9 Å, b = 3.9 Å. Such lattice parameter is similar to but has a certain distortion from the bulk crystals. It is reasonable owing to the flexible nature of alkane chain and the fast crystal formation process.

3.2. Morphology and transistor of pentacene/$C_{44}H_{90}$

It is a natural step to consider the application of such large ultra-thin 2D crystals acting as good molecular templates for the growth of highly ordered organic semiconductor crystalline films, and for achieving better device performance [28,44–46]. Hence we choose the benchmark organic semiconductor pentacene to evaluate the possibility [47]. Fig. 4a–c shows the AFM morphologies of pentacene with varied thicknesses grown on the $C_{44}H_{90}$ monolayer crystals. Morphology of pentacene on bare SiO_2 was also recorded for comparison (Fig. 4d–f). At the early stage, the pentacene forms into typical fractal islands on the bare SiO_2, while on the $C_{44}H_{90}$ 2D crystals it changes to the quadrilateral-like island with even smaller size (Fig. 4a and d). With the

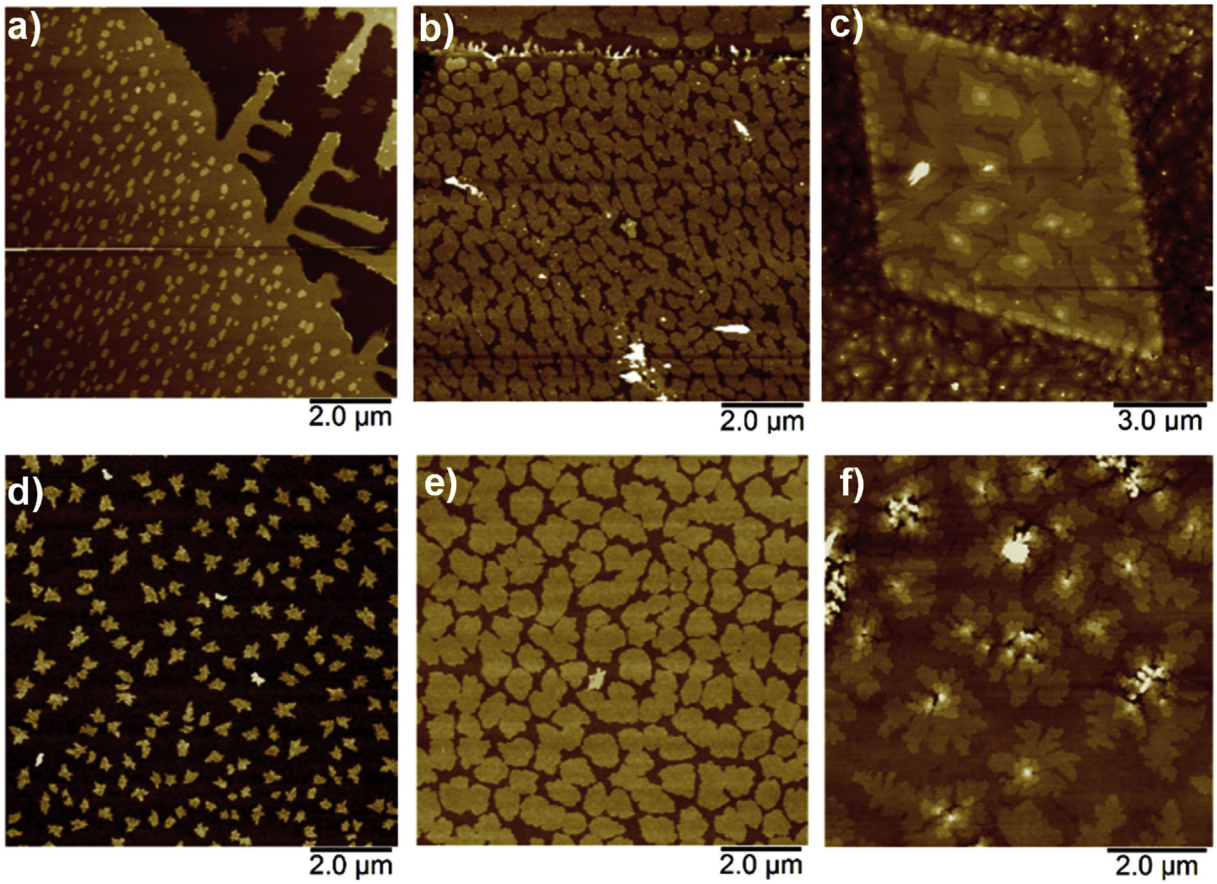

Fig. 4. a-c) pentacene film with different thicknesses grown on top of the $C_{44}H_{90}$ crystals d-f) pentacene film with different thicknesses grown on bare SiO_2/Si surface.

increase of the pentacene coverage, the size of these islands grow and coalescence with adjacent grains in both cases (Fig. 4b and e). It is interesting to note that for the thicker pentacene film, for example 10 nm (Fig. 4c and f), the morphologies are different on different surfaces. On $C_{44}H_{90}$ the small quadrilateral-like islands become larger and formed into highly ordered terraced-like film. In contrast, the fractal island on bare SiO_2 transformed into terraced islands with many screw dislocation defects [47–49]. The almost absence of the screw dislocation defect and the larger grain size of pentacene on the $C_{44}H_{90}$ modified area can be attributed to several reasons. Firstly, the diffusion ability of pentacene on $C_{44}H_{90}$ crystal decreases and this results in the high nucleation density and small grain size initially which is benefit to avoid the formation of dislocations [49]. Secondly, owing to the single crystal surface of $C_{44}H_{90}$, the pentacene grains tend to form preferred orientations owing to the template effect [28]. We characterized the packing of pentacene on top of $C_{44}H_{90}$ crystals using high resolution AFM, an good alignment between the two molecules was observed (Fig. S3). While it is also note that multiple orientations exists. The detailed orientation information and the lattice relationship between pentacene and $C_{44}H_{90}$ have to be further determined in the future. The adjacent domains with similar alignment coalesce and produce large domains with increased film thickness. According to the XRD results (Fig. S4), the pentacene packing is similar in both films. Nevertheless, the highly ordered pentacence films on the 2D crystal surface should offer a better charge transport ability.

To evaluate the charge transport property of the pentacene films, we fabricated the thin film transistor devices based on the pentacene/$C_{44}H_{90}$ films and presented the performance in Fig. 5a and b. The device shows a higher hole mobility of 0.49 $cm^2 V^{-1}s^{-1}$. In contrast, under the same preparation conditions, the pentacene transistor on bare SiO_2 exhibits a mobility only about 0.064 $cm^2 V^{-1}s^{-1}$ (Fig. 5c and d). The repeated experiments give mobilities of pentacene/$C_{44}H_{90}$ in the range from 0.2 to 0.5 $cm^2 V^{-1}s^{-1}$, while of the pentacene without $C_{44}H_{90}$ is 0.03–0.1 $cm^2 V^{-1}s^{-1}$. In addition, since the $C_{44}H_{90}$ crystals only cover part of the channel, the true mobility for pentacene on the 2D crystals should be even higher than the presented results. While since here pentacene film is still polycrystalline that it does not have obvious anisotropic transport behavior. On one hand, the significant improvement of the charge mobility could be attributed to the improved morphology, specifically the decrement of the dislocation defects; on the other hand, it should also benefit from the passivation effect of $C_{44}H_{90}$ crystals on the SiO_2 surface [44]. To figure out such issue, we conducted the Kelvin probe force microscopy (KPFM) to check the interface information. KPFM of two samples, the $C_{44}H_{90}$ on SiO_2, pentacene on $C_{44}H_{90}/SiO_2$ were measured and depicted in Fig. 6 (a and c are the height image, b and d are the surface potential image). When the SiO_2 is only covered with $C_{44}H_{90}$, we find that the contact potential difference (CPD) of $C_{44}H_{90}$ is similar to the adjacent bare SiO_2 surface (Fig. 6a and b). This is because both SiO_2 and $C_{44}H_{90}$ are insulating materials without obvious inherent dipole. These surfaces have low charge density or induced charge density, leading to the similar surface potential. However, when the pentacene films are deposited, obvious different CPD signals appeared for the pentacene on SiO_2 and that on $C_{44}H_{90}$ crystals (Fig. 6c and d). The pentacene domains locating on the $C_{44}H_{90}$ area present significantly lower CPD than those on the bare SiO_2. Such difference could attribute to two reasons. On one hand, an interface dipole at the interface between pentacene and $C_{44}H_{90}$ might exist. On the other hand, as we know, many –OH group exists on the SiO_2 surface, which could attract and trap the holes on the organic/insulator interface and decreases the mobility. If the $C_{44}H_{90}$ is covered in prior, the above effect is eliminated or reduced. This passivation could significantly reduce the –OH influence on the charge trapping and

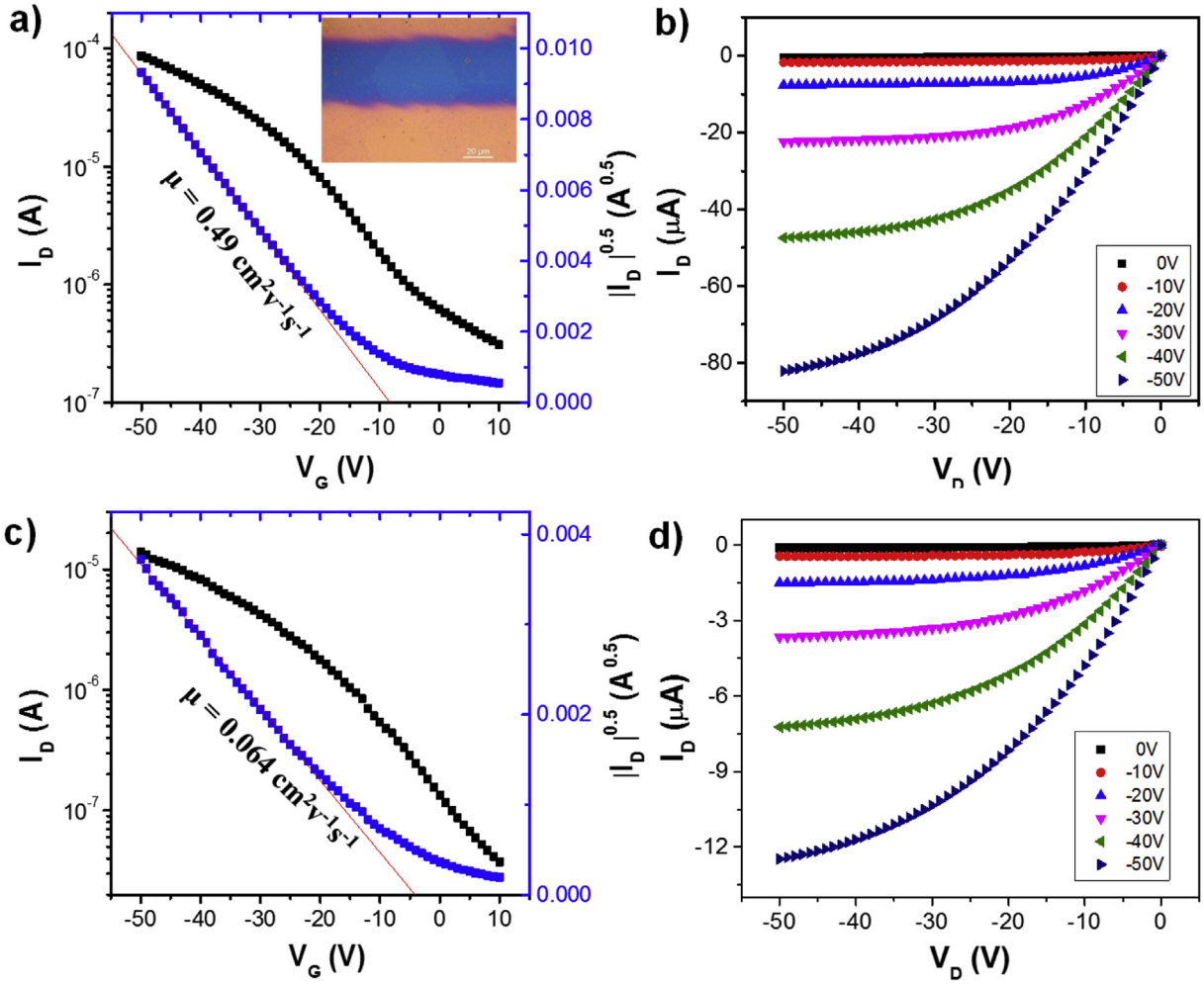

Fig. 5. The transistor performance of pentacene on top of the $C_{44}H_{90}$ crystals and on bare SiO_2/Si substrates. a-b) on substrates with $C_{44}H_{90}$ crystals, c-d) on bare SiO_2/Si.

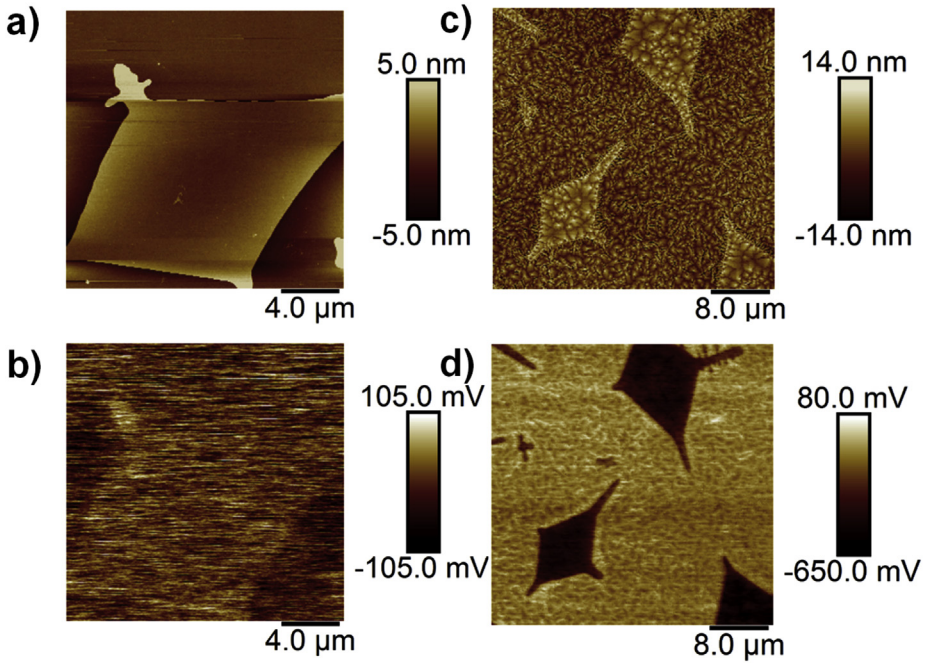

Fig. 6. The height and surface potential images of a-b) $C_{44}H_{90}/SiO_2$/Si, c-d) pentacene on $C_{44}H_{90}/SiO_2$/Si.

improve the charge transport of pentacene film, leading to a better performance.

4. Conclusions

In conclusion, we have realized the formation of monolayer 2D molecular crystals with regular quadrangular shape via a fast dip-coating method and obtained the clear packing model of such crystals. These 2D crystals randomly dispersed on the substrate and exhibited a speed dependent size varied from several micrometers to hundreds of micrometers. The formation of such 2D crystal is benefited with the low solubility of $C_{44}H_{90}$ and isotropic Van der Waals interaction under the entrainment regime of the typical dip-coating process. In addition, these smooth 2D crystals show promising application in the thin film transistors by acting as a molecular template layer. The modified pentacene film transistor presented an improvement on the charge mobility by about one magnitude owing to the decrease of the screw dislocation defects and passivation of trapping on the dielectric surface.

Acknowledgement

The authors acknowledge financial support from the National Natural Science Foundation of China (Grant Nos., 51503138, 51773143 and 21527805), China Postdoctoral Science Foundation (Grant Nos. 2014M550304, 2015M581856 and 2015T80579), Postdoctoral Science Foundation of Jiangsu Province (Grant No. 1501022A), University Science Research Project of Jiangsu Province (17KJB430027), and Open Research Fund of State Key Laboratory of Polymer Physics and Chemistry, Changchun Institute of Applied Chemistry, Chinese Academy of Sciences (201516). The authors also acknowledge the support from the Collaborative Innovation Center of Suzhou Nano Science & Technology and the Priority Academic Program Development of Jiangsu Higher Education Institutions. The authors thank those associated with beamline BL14B1 (Shanghai Synchrotron Radiation Facility) for providing the beam time.

Appendix A. Supplementary data

Supplementary data related to this article can be found at http://dx.doi.org/10.1016/j.orgel.2018.03.038.

References

[1] J.M. Lehn, Toward self-organization and complex matter, Science 295 (2002) 2400–2403.
[2] R.J. Li, W.P. Hu, Y.Q. Liu, D.B. Zhu, Micro- and nanocrystals of organic semiconductors, Acc. Chem. Res. 43 (2010) 529–540.
[3] F. Yang, S. Cheng, X. Zhang, X. Ren, R. Li, H. Dong, W. Hu, 2D organic materials for optoelectronic applications, Adv. Mater. 30 (2018) 1702415.
[4] A.L. Briseno, J. Aizenberg, Y.J. Han, R.A. Penkala, H. Moon, A.J. Lovinger, C. Kloc, Z.A. Bao, Patterned growth of large oriented organic semiconductor single crystals on self-assembled monolayer templates, J. Am. Chem. Soc. 127 (2005) 12164–12165.
[5] C.Y. Zhang, X.J. Zhang, X.H. Zhang, X.M. Ou, W.F. Zhang, J.S. Jie, J.C. Chang, C.S. Lee, S.T. Lee, Facile one-step fabrication of ordered organic nanowire films, Adv. Mater. 21 (2009) 4172–4176.
[6] A. Kumatani, C. Liu, Y. Li, P. Darmawan, K. Takimiya, T. Minari, K. Tsukagoshi, Solution-processed, self-organized organic single crystal arrays with controlled crystal orientation, Sci. Rep. 2 (2012) 393.
[7] A. Kim, K.S. Jang, J. Kim, J.C. Won, M.H. Yi, H. Kim, D.K. Yoon, T.J. Shin, M.H. Lee, J.W. Ka, Y.H. Kim, Solvent-free directed patterning of a highly ordered liquid crystalline organic semiconductor via template-assisted self-assembly for organic transistors, Adv. Mater. 25 (2013) 6219–6225.
[8] C.Y. Xiao, X.N. Kan, C.M. Liu, W. Jiang, G.Y. Zhao, Q. Zhao, L. Zhang, W.P. Hu, Z.H. Wang, L. Jiang, Controlled formation of large-area single-crystalline TIPS-pentacene arrays through superhydrophobic micropillar flow-coating, J. Mater. Chem. C 5 (2017) 2702–2707.
[9] Q.J. Wang, J. Qian, Y. Li, Y.H. Zhang, D.W. He, S. Jiang, Y. Wang, X.R. Wang, L.J. Pan, J.Z. Wang, X.Z. Wang, Z. Hu, H.Y. Nan, Z.H. Ni, Y.D. Zheng, Y. Shi, 2D single-crystalline molecular semiconductors with precise layer definition achieved by floating-coffee-ring-driven assembly, Adv. Funct. Mater. 26 (2016) 3191–3198.
[10] S. Das, R. Gulotty, A.V. Sumant, A. Roelofs, All two-dimensional, flexible, transparent, and thinnest thin film transistor, Nano Lett. 14 (2014) 2861–2866.
[11] J.Z. Ou, W.Y. Ge, B. Carey, T. Daeneke, A. Rotbart, W. Shan, Y.C. Wang, Z.Q. Fu, A.F. Chrimes, W. Wiodarski, S.P. Russo, Y.X. Li, K. Kalantar-zadeh, Physisorption-based charge transfer in two-dimensional SnS2 for selective and reversible NO2 gas sensing, ACS Nano 9 (2015) 10313–10323.
[12] M. Zhao, F.X. Yang, C. Liang, D.W. Wang, D.F. Ding, J.W. Lv, J.Q. Zhang, W.P. Hu, C.G. Lu, Z.Y. Tang, High hole mobility in long-range ordered 2D lead sulfide nanocrystal monolayer films, Adv. Funct. Mater. 26 (2016) 5182–5188.
[13] G. Giri, E. Verploegen, S.C.B. Mannsfeld, S. Atahan-Evrenk, D.H. Kim, S.Y. Lee, H.A. Becerril, A. Aspuru-Guzik, M.F. Toney, Z.A. Bao, Tuning charge transport in solution-sheared organic semiconductors using lattice strain, Nature 480 (2011) 504–U124.
[14] H.B. Akkerman, A.C. Chang, E. Verploegen, C.J. Bettinger, M.F. Toney, Z.N. Bao, Fabrication of organic semiconductor crystalline thin films and crystals from solution by confined crystallization, Org. Electron. 13 (2012) 235–243.
[15] H.B. Akkerman, H.Y. Li, Z.N. Bao, TIPS-pentacene crystalline thin film growth, Org. Electron. 13 (2012) 2056–2062.
[16] S.H. Wang, W. Pisula, K. Mullen, Nanofiber growth and alignment in solution processed n-type naphthalene-diimide-based polymeric field-effect transistors, J. Mater. Chem. 22 (2012) 24827–24831.
[17] R.R. Bao, C.Y. Zhang, X.J. Zhang, X.M. Ou, C.S. Lee, J.S. Jie, X.H. Zhang, Self-Assembly, Hierarchical Patterning, Of aligned organic nanowire arrays by solvent evaporation on substrates with patterned wettability, ACS Appl. Mater. Interfaces 5 (2013) 5757–5762.
[18] J.J. Chang, C.Y. Chi, J. Zhang, J.S. Wu, Controlled growth of large-area high-performance small-molecule organic single-crystalline transistors by slot-die coating using a mixed solvent system, Adv. Mater. 25 (2013) 6442–6447.
[19] C.C. Fan, A.P. Zoombelt, H. Jiang, W.F. Fu, J.K. Wu, W.T. Yuan, Y. Wang, H.Y. Li, H.Z. Chen, Z.N. Bao, Solution-grown organic single-crystalline p-n junctions with ambipolar charge transport, Adv. Mater. 25 (2013) 5762–5766.
[20] D.T. James, J.M. Frost, J. Wade, J. Nelson, J.S. Kim, Controlling microstructure of pentacene derivatives by solution processing: impact of structural anisotropy on optoelectronic properties, ACS Nano 7 (2013) 7983–7991.
[21] N. Shin, J. Kang, L.J. Richter, V.M. Prabhu, R.J. Kline, D.A. Fischer, D.M. DeLongchamp, M.F. Toney, S.K. Satija, D.J. Gundlach, B. Purushothaman, J.E. Anthony, D.Y. Yoon, Vertically segregated structure and properties of small molecule-polymer blend semiconductors for organic thin-film transistors, Adv. Funct. Mater. 23 (2013) 366–376.
[22] M. Park, Y. Min, Y.J. Lee, U. Jeong, Growth of long triisopropylsilylethynyl pentacene (TIPS-PEN) nanofibrils in a polymer thin film during spin-coating, Macromol. Rapid Commun. 35 (2014) 655–660.
[23] Y. Wang, L. Chen, Q.J. Wang, H.B. Sun, X.Z. Wang, Z. Hu, Y. Li, Y. Shi, Solution-processed organic crystals written directly with a rollerball pen for field-effect transistors, Org. Electron. 15 (2014) 2234–2239.
[24] J. Jang, S. Nam, K. Im, J. Hur, S.N. Cha, J. Kim, H.B. Son, H. Suh, M.A. Loth, J.E. Anthony, J.J. Park, C.E. Park, J.M. Kim, K. Kim, Highly crystalline soluble acene crystal arrays for organic transistors: mechanism of crystal growth during dip-coating, Adv. Funct. Mater. 22 (2012) 1005–1014.
[25] L.Q. Li, P. Gao, W.C. Wang, K. Mullen, H. Fuchs, L.F. Chi, Growth of ultrathin organic semiconductor microstripes with thickness control in the monolayer precision, Angew. Chem. Int. Ed. 52 (2013) 12530–12535.
[26] M.M. Li, C.B. An, W. Pisula, K. Mullen, Alignment of organic semiconductor microstripes by two-phase dip-coating, Small 10 (2014) 1926–1931.
[27] B.H. Wang, T. Zhu, L.Z. Huang, T.L.D. Tam, Z.Q. Cui, J.Q. Ding, L.F. Chi, Addressable growth of oriented organic semiconductor ultra-thin films on hydrophobic surface by direct dip-coating, Org. Electron. 24 (2015) 170–175.
[28] J.L. Yang, D.H. Yan, T.S. Jones, Molecular template growth and its applications in organic electronics and optoelectronics, Chem. Rev. 115 (2015) 5570–5603.
[29] K.J. Wu, H.W. Li, L.Q. Li, S.N. Zhang, X.S. Chen, Z.Y. Xu, X. Zhang, W.P. Hu, L.F. Chi, X.K. Gao, Y.C. Meng, Controlled growth of ultrathin film of organic semiconductors by balancing the competitive processes in dip-coating for organic transistors, Langmuir 32 (2016) 6246–6254.
[30] T. Zhu, C.L. Xiao, B.H. Wang, X.R. Hu, Z. Wang, J. Fan, L.Z. Huang, D.H. Yang, L.F. Chi, Growth of highly oriented ultrathin crystalline organic microstripes: effect of alkyl chain length, Langmuir 32 (2016) 9109–9117.
[31] T.P. Corrales, M.J. Bai, V. del Campo, P. Homm, P. Ferrari, A. Diama, C. Wagner, H. Taub, K. Knorr, M. Deutsch, M.J. Retamal, U.G. Volkmann, P. Huber, Spontaneous formation of nanopatterns in velocity-dependent dip-coated organic films: from dragonflies to stripes, ACS Nano 8 (2014) 9954–9963.
[32] Y. Huang, J. Sun, J. Zhang, S. Wang, H. Huang, J. Zhang, D. Yan, Y. Gao, J. Yang, Controllable thin-film morphology and structure for 2,7-dioctyl[1]benzothieno[3,2-b][1]benzothiophene (C8BTBT) based organic field-effect transistors, Org. Electron. 36 (2016) 73–81.
[33] W. Huang, B. Yang, J. Sun, B. Liu, J. Yang, Y. Zou, J. Xiong, C. Zhou, Y. Gao, Organic field-effect transistor and its photoresponse using a benzo[1,2-b:4,5-b′]difuran-based donor–acceptor conjugated polymer, Org. Electron. 15 (2014) 1050–1055.
[34] L. Li, P. Gao, M. Baumgarten, K. Müllen, N. Lu, H. Fuchs, L. Chi, High performance field-effect ammonia sensors based on a structured ultrathin organic semiconductor film, Adv. Mater. 25 (2013) 3419–3425.
[35] X. Zhang, C.H. Hsu, X. Ren, Y. Gu, B. Song, H.J. Sun, S. Yang, E. Chen, Y. Tu, X. Li, X. Yang, Y. Li, X. Zhu, Supramolecular [60]fullerene liquid crystals formed by self-organized two-dimensional crystals, Angew. Chem. Int. Ed. 54 (2015) 114–117.
[36] L. Jiang, H. Dong, Q. Meng, H. Li, M. He, Z. Wei, Y. He, W. Hu, Millimeter-sized molecular monolayer two-dimensional crystals, Adv. Mater. 23 (2011) 2059–2063.
[37] M. Faustini, B. Louis, P.A. Albouy, M. Kuemmel, D. Grosso, Preparation of sol-gel

films by dip-coating in extreme conditions, J. Phys. Chem. C 114 (2010) 7637–7645.
[38] B.M. Ocko, X.Z. Wu, E.B. Sirota, S.K. Sinha, O. Gang, M. Deutsch, Surface freezing in chain molecules: normal alkanes, Phys. Rev. E 55 (1997) 3164–3182.
[39] P. Lazar, H. Schollmeyer, H. Riegler, Spreading and two-dimensional mobility of long-chain alkanes at solid/gas interfaces, Phys. Rev. Lett. 94 (2005) 116101.
[40] P.W. Teare, The crystal structure of orthorhombic hexatriacontane, C36H74, Acta Crystallogr. 12 (1959) 294–300.
[41] A. Holzwarth, S. Leporatti, H. Riegler, Molecular ordering and domain morphology of molecularly thin triacontane films at SiO2/air interfaces, EPL (Europhys. Lett.) 52 (2000) 653.
[42] J.-P. Gorce, S.J. Spells, X.-B. Zeng, G. Ungar, Infrared active methyl group vibrations in tetratetracontane: a probe for chain end organization and crystal structure, J. Phys. Chem. B 108 (2004) 3130–3139.
[43] M. Bai, K. Knorr, M.J. Simpson, S. Trogisch, H. Taub, S.N. Ehrlich, H. Mo, U.G. Volkmann, F.Y. Hansen, Nanoscale observation of delayering in alkane films, EPL (Europhys. Lett.) 79 (2007) 26003.
[44] L.Y. Xiang, W. Wang, F.L. Gao, Improving mobility and stability of organic field-effect transistors by employing a tetratetracontane modifying PMMA dielectric, IEEE Electron. Dev. 63 (2016) 4440–4444.
[45] L.Y. Xiang, J. Ying, W. Wang, W.F. Xie, High mobility n-channel organic field-effect transistor based a tetratetracontane interfacial layer on gate dielectrics, IEEE Electr. Dev. 37 (2016) 1632–1635.
[46] S. Ogawa, Y. Kimura, M. Niwano, H. Ishii, Trap elimination and injection switching at organic field effect transistor by inserting an alkane (C44H90) layer, Appl. Phys. Lett. 90 (2007) 033504.
[47] C.D. Dimitrakopoulos, A.R. Brown, A. Pomp, Molecular beam deposited thin films of pentacene for organic field effect transistor applications, J. Appl. Phys. 80 (1996) 2501–2508.
[48] Y.Y. Lin, D.J. Gundlach, S.F. Nelson, T.N. Jackson, Stacked pentacene layer organic thin-film transistors with improved characteristics, IEEE Electron. Device Lett. 18 (1997) 606–608.
[49] R. Ruiz, B. Nickel, N. Koch, L.C. Feldman, R.F. Haglund, A. Kahn, G. Scoles, Pentacene ultrathin film formation on reduced and oxidized Si surfaces, Phys. Rev. B 67 (2003).